



Substitutional carbon-dioxygen center in irradiated silicon

M.S. Potsidi ^{a,*}, N. Kuganathan ^{b,c}, A. Chroneos ^{b,c}, S.-R.G. Christopoulos ^b, T. Angeletos ^a, N. V. Sarlis ^a, C.A. Londos ^{a,**}

^a National and Kapodistrian University of Athens, Department of Physics, Section of Condensed Matter Physics, Panepistimiopolis Zografos, Athens, 157 84, Greece

^b Faculty of Engineering, Environment and Computing, Coventry University, Priory Street, Coventry, CV1 5FB, UK

^c Department of Materials, Imperial College London, London, SW7 2AZ, UK



ARTICLE INFO

Keywords:
Silicon
Irradiation
IR spectroscopy
DFT calculations

ABSTRACT

This work reports theoretical and experimental studies of the substitutional carbon-dioxygen (C_sO_{2i}) defect in silicon (Si). To this end, density functional theory (DFT) calculations were used to predict the lowest energy structure of the defect. Thereafter, the dipole-dipole interaction method was employed to calculate the local vibration modes (LVM) of this lowest energy structure. We found that the C_sO_{2i} defect is characterized by two LVM frequencies at 1064.7 and 1140.1 cm^{-1} . These values are quite close to experimental bands of earlier studies at 1048 and 1094 cm^{-1} (deviation ~1.6 and 4.2%) reported in the literature, both attributed to the C_sO_{2i} defect. Next, infrared Spectroscopy (IR) measurements were carried, out at room temperature (RT), on electron irradiated Si samples. A band at 1048 cm^{-1} was observed. It is grown in the spectra upon annealing out of the 830 cm^{-1} band of the vacancy-oxygen center (VO) and the 861 cm^{-1} band of the carbon interstitial-oxygen interstitial center (C_iO_i). Furthermore, isochronal anneals were carried out to monitor the evolution of the band. The analysis and examination of the results lead us to suggest that the 1048 cm^{-1} band originates from the C_sO_{2i} complex, formed according to the reaction: $VO + C_iO_i \rightarrow C_sO_{2i}$. The other band at 1094 cm^{-1} is most probably masked by the very strong band of O_i (1107 cm^{-1} , at RT) in Si.

1. Introduction

As silicon (Si) is a key material in the semiconductor industry (optoelectronics, nanoelectronics, solar cells and sensors) its quality is important for the functionality of devices. This is affected by impurities and defects introduced in the lattice, in the course of material growth and/or of material processing [1–6]. The understanding of the structure, properties and behavior of defects in Si is highly significant, both for scientific and technological reasons [1,2].

Oxygen (O) and carbon (C) are the most common impurities unintentionally introduced in the Si lattice, during crystal growth and device processing [7–10]. Although both are electrically inert in the Si lattice (oxygen as an interstitial, (O_i) and carbon as a substitutional, (C_s)), they can affect the electrical properties of Si upon material possessing through the formation of various complexes (for example, thermal donors and oxygen precipitates created upon thermal treatments) [7,8, 11–14]. Additionally, the C and O impurities lead to the formation of a number of complexes upon irradiation and/or implantation. Important,

among them, are the vacancy-oxygen (VO), the carbon interstitial-oxygen interstitial (C_iO_i) and carbon interstitial-carbon substitutional (C_iC_s) pairs, which are electrical active and introduce levels in the Si lattice [7,8]. Their presence leads to performance losses and degradation of the devices [15–24]. Furthermore, upon annealing these defects participate in a variety of reaction channels leading to the formation of numerous second generation complexes.

Here, we focus on carbon-oxygen defects and in particular on the carbon substitutional-dioxygen defect (C_sO_{2i}). This complex has been detected in a number of experiments, under different conditions of irradiations carried out at various temperatures. Previous studies have detected two IR bands at 1052 and 1099 cm^{-1} measured at low temperature and were attributed to a C–O complex [25]. These bands were later correlated with the C_sO_{2i} complex, and in particular with two oxygen-related LVMs of its structure [26–28]. C_sO_{2i} is a second order generation defect and one way to form is by the interaction of the VO and the C_iO_i pairs, upon their annealing around 300 °C [29,30]. The suggested reaction is: $VO + C_iO_i \rightarrow C_sO_{2i}$. Notably, although VO and C_iO_i

* Corresponding author.

** Corresponding author.

E-mail addresses: mpotsidi@phys.uoa.gr (M.S. Potsidi), hlontos@phys.uoa.gr (C.A. Londos).

anneal out mainly by dissociation, a small percentage of them could migrate as entities and upon their encounter produce the C_sO_{2i} complex [7,31]. In this scheme, vacancies liberated from the dissociation of VO react with C_iO_i to form in the first place C_sO_i pairs, which then capture O_i from the dissociated C_iO_i pair to form finally C_sO_{2i} . The latter center could also be produced by the reaction $C_i + VO_2 \rightarrow C_sO_{2i}$, were carbon interstitial atoms (C_i) are produced by the liberation of the C_iO_i and vacancy-dioxygen centers (VO_2) are formed as a result of the VO annealing ($VO + O_i \rightarrow VO_2$) [32]. The same reaction was suggested for irradiations at 400–600 °C [33,34]. The 1052 and 1099 cm⁻¹ bands have also been reported in thermally treated Si material, were it was suggested that the capture of oxygen dimers (O_{2i}) by C_s impurities could lead to the formation of the C_sO_{2i} complex ($C_s + O_{2i} \rightarrow C_sO_{2i}$) [35]. We note that, in RT measurements the two bands of the complex shift to the values 1048 and 1094 cm⁻¹ [36].

In the present study, we investigate the lowest energy configuration of the C_sO_{2i} defect using DFT calculations. This structure is then used in dipole-dipole interaction method to calculate the LVM frequencies of the C_sO_{2i} structure. These were compared with IR spectroscopy measurements.

2. Methodology

2.1. Experimental methodology

We used Czochralski (Cz-Si) prepolished samples with typical dimensions of $15 \times 10 \times 1.8$ mm³. The samples, purchased from MEMC, were initially p-type (boron doped) with resistivity $\rho \sim 10 \Omega \text{ cm}$. The initial oxygen and carbon concentrations were $[O_i] = 1 \times 10^{18}$ and $[C_s] = 1.6 \times 10^{17}$ cm⁻³, respectively. Float-zone (FZ) samples of $[O_i] = 1 \times 10^{16}$ cm⁻³ and $[C_s]$ below detection limits were also used for comparison purposes. The Cz-Si samples were irradiated with 2 MeV electrons with a fluence of 1×10^{18} cm⁻² at about 80 °C, using the Dynamitron accelerator at Takasaki-JAERI (Japan). After irradiation the samples were subjected to isochronal anneals up to ~600 °C in open furnaces, in steps of ~10 °C and 20 min duration. After each annealing step, IR spectra were recorded at RT by means of a Fourier Transform Infrared spectrometer (JASCO-470 plus) with a resolution of 1 cm⁻¹. The two phonon absorption was always subtracted from each spectrum by using a reference sample of equal thickness from FZ material.

2.2. Theoretical methodology

Spin-polarised DFT calculations as implemented in the VASP code were used [37,38]. This code uses plane wave basis sets and projected augmented wave (PAW) potentials to solve the standard Kohn-Sham (KS) equations [39]. All calculations were performed using a supercell ($a = b = c = 19.3$ Å and $\alpha = \beta = \gamma = 60^\circ$) consisting of 250 Si atoms. The generalized gradient approximation (GGA) as parameterised by Perdew, Burke and Ernzerhof (PBE) was used to model the exchange correlation effects [40]. A plane wave basis set with a cut-off of 500 eV and a $2 \times 2 \times 2$ Monkhorst-Pack k-point mesh which yielded 8 irreducible k-points were used [41]. Geometry optimisations were performed under constant pressure conditions (both positions of atoms and lattice parameters were relaxed simultaneously) with the aid of a conjugate gradient algorithm [42]. All optimised configurations reached the required accuracy of convergence (force tolerance 0.01 eV/Å and stress tensor 0.002 GPa). Bader charge analysis as implemented in the VASP code was carried out to determine the charges on the C, Si and O atoms [43]. The dispersion interactions were included in a semi-empirical form as implemented by Grimme et al. [44]. The efficacy of electronic structure simulations to model group IV semiconductors and the importance of related defects has been demonstrated in previous works [45–48].

3. Results and discussion

Before proceeding, in order to be an agreement between the notation of DFT outcomes and that used in the dipole–dipole analysis, we will make a few remarks. When used, C refers to the C_s defect, O_1 or $O_{i(1)}$ stand for the oxygen interstitial atom in the C_sO_i defect and O_2 or $O_{i(2)}$ stand for the second oxygen interstitial atom in the final C_sO_{2i} defect.

Fig. 1a displays three characteristic IR spectra of the Cz-Si samples, in the frequency range 800–1075 cm⁻¹. All spectra were taken after irradiation. The lower one was recorded immediately after irradiation, prior to annealing. The middle was recorded after irradiation and the 200 °C annealing step (the successive isochronal anneal sequence consisted of ~10 °C/20min steps). Similarly, the upper one was recorded after irradiation and the 350 °C annealing step of the same anneal sequence. In this frequency range we observe LVM bands of well-known defects as VO (830 cm⁻¹), C_iO_i (861 cm⁻¹), $C_iO_i(Si)$ (936, 1020 cm⁻¹) after irradiation (lower curve), and VO_2 (888 cm⁻¹), as well as bands at 1020 and 1048 cm⁻¹ at 350 °C (upper curve). **Fig. 1b** depicts the IR spectrum after irradiation and subsequent annealing at 350 °C in the frequency range 650–1200 cm⁻¹, so that it includes region around the intense line of oxygen interstitial at 1107 cm⁻¹. The band at 1020 cm⁻¹ in the upper curve of **Fig. 1(a)** is different from that at 1020 cm⁻¹ of the lower curve, originated from the $C_iO_i(Si)$ complex and annealed out at

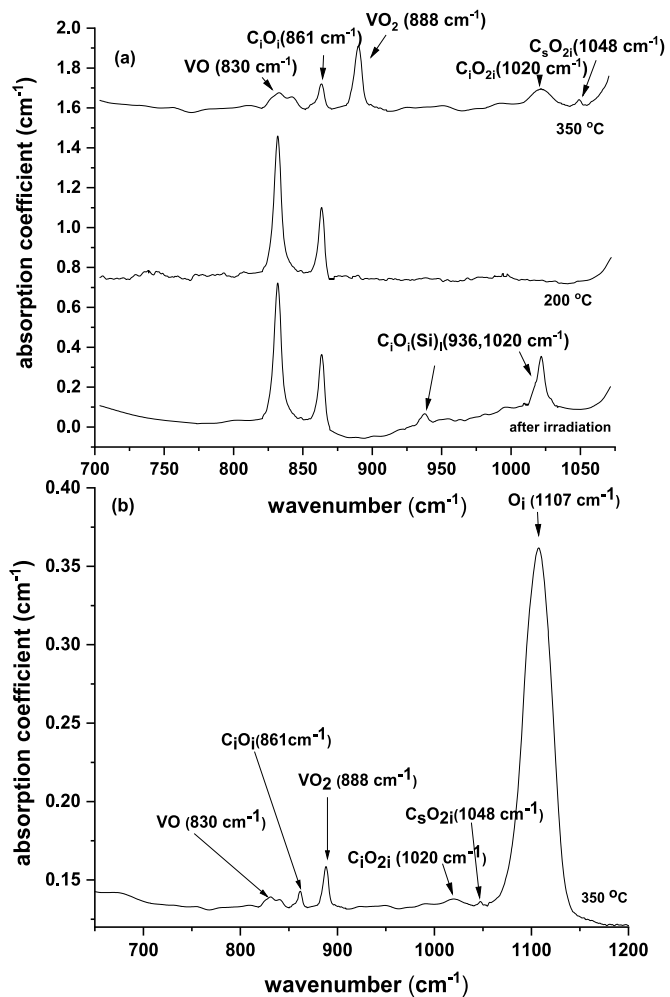


Fig. 1. (a) Characteristic segments of the IR spectra of the Cz-Si samples after irradiation (lower curve), after irradiation and the subsequent annealing step at 200 °C (middle curve) and after irradiation and the subsequent annealing step at 350 °C (upper curve). (b) The spectrum after irradiation and the subsequent annealing step at 350 °C, in the frequency range 650–1200 cm⁻¹.

~ 200 °C (see middle curve) [49]. The investigation of the latter band at 1048 cm⁻¹ is the main aim of this work.

Fig. 2 demonstrates the evolution with temperature of the VO, C_iO_i, VO₂ and 1048 cm⁻¹ bands. 1048 cm⁻¹ band seems to arise in the spectra upon annealing out of the VO and the C_iO_i defects. It has been correlated with the C_sO_{2i} complex [26–29]. In the work below, we have used theoretical results employing DFT and dipole-dipole approximation methods, which we combined with experimental results from IR spectroscopy to investigate the above attribution.

3.1. The carbon substitutional (C_i) defect in Si

First, we considered the single-carbon doped silicon, the relaxed structure of which is shown in **Fig. 3a**. **Table 1** (see Appendix) lists the calculated bond distances and bond angles near the defect. Doping introduces a small distortion in the lattice with the formation of shorter Si-C bonds (~2.00 Å) than the Si-Si bonds calculated in bulk silicon (2.36 Å) (refer to **Table 1**) and displacement of Si atom towards dopant. Furthermore, there is a slight perturbation in the Si-Si bond distances around the defect (refer to **Table 1**). The bond angles (Si-Si-Si) in a tetrahedral Si₄ unit in the Si are calculated to be 109.3°–109.6°.

These values do not deviate much from those calculated in the CSi₃ tetrahedral unit. In the tetrahedral unit formed by the displaced Si atom (Si₁CSi₈Si₁₁), there is a slight elongation in the bond lengths (2.40 Å) and a significant reduction in the bond angles (102.5°) due to the upward movement of Si. Bader charge on the doped C is –4.11 showing the significant electron gain from the nearest neighbor Si atoms. This is further evidenced by the positive Bader charges (4 × ~1.00) on the four Si atoms attached to the C. This is clearly due to the higher electronegativity of C (2.55) than that of Si (1.90) [50].

3.2. The carbon substitutional-dioxygen center (C_sO_{2i})

Next, we considered the oxygen di-interstitials in carbon-doped silicon (C_sO_{2i} defect). The optimised structure is shown in **Fig. 4**, the density of states (DOS) and charge density plots are shown in **Fig. 5**.

The selected bond distances and bond angles retrieved from the relaxed structure are shown in **Fig. 6** in the LVM band estimation section (see below). Each oxygen atom is bonded to two Si atoms in which one of them is directly bonded to C. The Si₃C tetrahedral unit exhibits shorter Si-C bond distances as discussed earlier. Interestingly, the Si₁-C bond distance is shorter by ~0.1 Å than that calculated in the tetrahedral unit

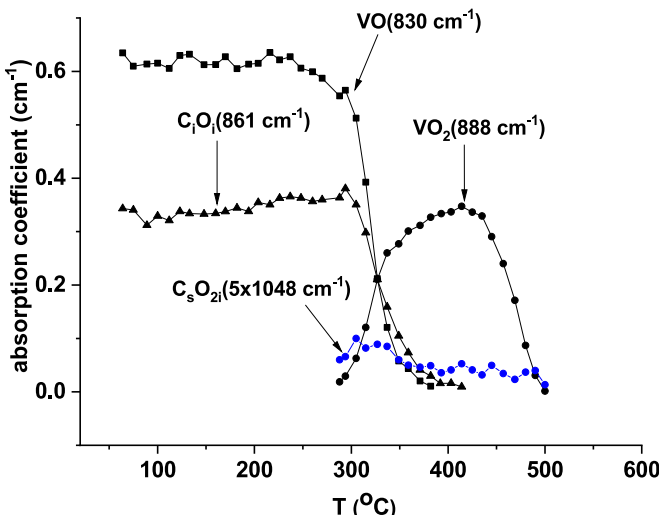


Fig. 2. Thermal evolution of the VO, C_iO_i, VO₂ defects and the 1048 cm⁻¹ band upon isochronal annealing up to ~ 500 °C. The absorption coefficient of 1048 cm⁻¹ line has been magnified by 5.

of C-doped silicon. This is clearly due to the high Bader charge of +3.01 on the Si₁ which forms strong bond with C. The amount of electrons on the C (~4.10) is donated by four Si atoms (4 × ~1.00). The rest of the Bader charge of +2.00 on the Si₁ is due its donation of one electron each to the interstitial O atoms. The remaining one electron for each oxygen atom form O²⁻ is donated by adjacent Si atoms (Si₈ and Si₉). Though the donation of one electron is directly from Si₈ to O₁, the electron donation from Si₉ is not straight forward. That donation is obviously from the Si₁₀ but via Si₉ as Si₁₀-O₂ bond distance is too long (2.63 Å) for the direct donation. Both oxygen interstitials form bent structures with adjacent Si atoms with the bond angles of 141.68° and 150.92°.

The total DOS plot (see **Fig. 5a**) shows that C-doped silicon is a semiconductor. The p-states of C are mainly located in the valence band showing the strong bonding nature of C with silicon bulk (see **Fig. 5b**). This is further confirmed by the total charge density plot and band decomposed charged density plot associated with C. Atomic DOS plots associated with interstitial oxygen show that p-states of oxygen atoms are strongly bound to silicon atoms they directly attached to and doped-C as evidenced by their band decomposed charged density plots.

LVM band estimation of the C_sO_{2i} defect via the Dipole-Dipole Interaction Method.

Fig. 6 demonstrates the lowest energy configuration of the C_sO_{2i} defect, in a unit cell, as derived from DFT calculations. The C_sO_{i(1)} and O_{i(2)} defects with reported effective charges [19] can be considered as two oscillating interacting dipoles. For the investigation of the LVM lines of C_sO_{2i} we have considered that the oxygen related line of C_sO_{i(1)} at 1103 cm⁻¹, reported in previous work [7], has been perturbed by the presence of a second oxygen interstitial atom (O_{i(2)}).

Regarding the C_sO_{i(1)} dipole, C_s and O_{i(1)} atoms are considered as one particle with mass equal to the reduced mass of oxygen and carbon atoms μ , located at the center of mass, at distance d from O_{i(1)} atom. The reduced mass μ is derived from the relation

$$\mu = \frac{m_O m_C}{m_O + m_C} \quad (1)$$

while the distance d from the relation

$$d = \frac{m_C}{m_O + m_C} d_{C_s O_{i(1)}} \quad (2)$$

where $m_O = 16$ amu, $m_C = 12$ amu are the masses of the oxygen and carbon atoms, respectively and $d_{C_s O_{i(1)}} = 2.817$ Å is the distance between the C_s and O_{i(1)} atoms. The calculated values for μ and d , are $\mu = 11.38 \cdot 10^{-27}$ kg and $d = 1.206$ Å, respectively. In order to estimate the LVM frequencies of a defect, it deserves at this point to refer on the defect effective charge, which is essential for the dipole-dipole model presented below. Importantly, the interaction between electromagnetic radiation and a defect in a crystal presuppose the existence of a dipole moment [9,51,52]. The effective charge expresses the dipole moment per unit displacement, in units of the electron charge, and is related to the coupling of the defect with the electric field of the electromagnetic radiation. In that case a band appears in the IR spectra at a certain frequency characterizing the LVM of the defect. The integrated absorption I of a LVM of an impurity is given by the relation

$$I = \int ad\omega \cong a_{max}\Delta = \frac{2\pi^2 Z^2}{n M_{imp} c} N \quad (3)$$

where a_{max} (in cm⁻¹) is the absorption coefficient and Δ is the full width at half maximum (in cm⁻¹) of the line, Z is the effective charge of the impurity, N the concentration of the impurity, n is the refractive index of the material, M_{imp} the mass of the impurity and c is the light velocity. Effective charges can be obtained both theoretically and experimentally. The effective charge associated with the defect and its immediate neighbors it generally difficult to be accurately calculated theoretically. However values of effective charges have been obtained for instance by ab initio local-density-functional cluster calculations by computing the

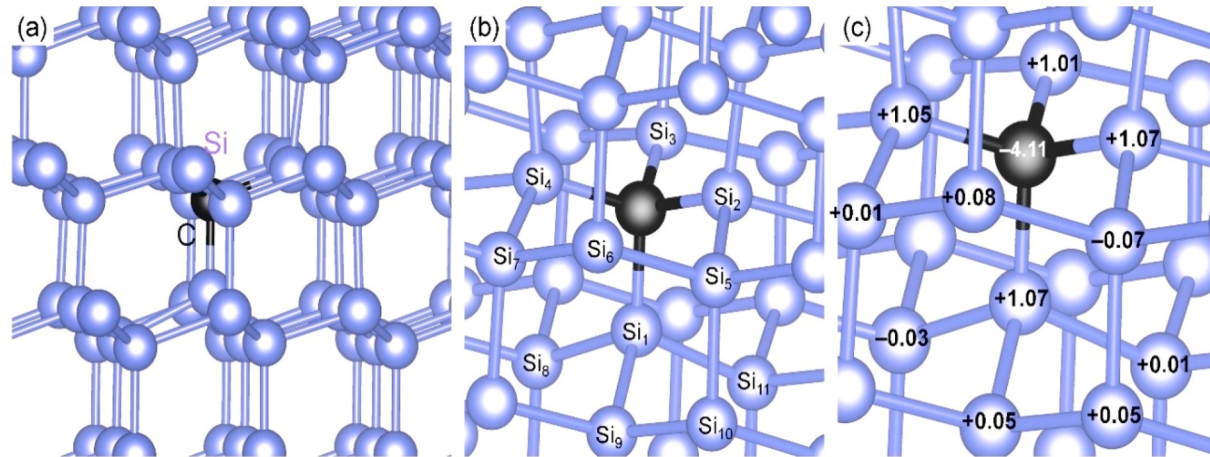


Fig. 3. (a) Relaxed structure of a single C-doped silicon, (b) a clear view of the defect structure and (c) Bader charges on the atoms near the defect.

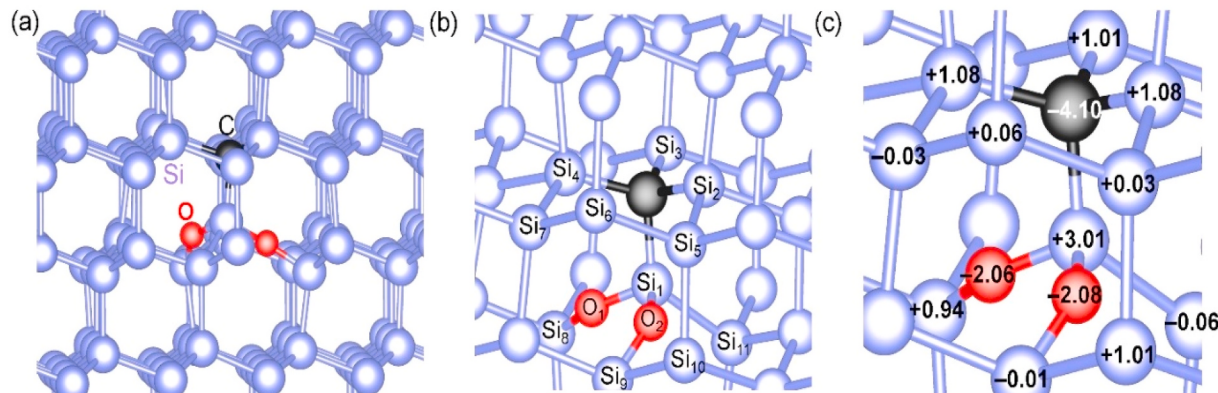


Fig. 4. The C_sO_{2i} defect. (a) Relaxed structure of oxygen di-interstitials at a single C-doped silicon, (b) a clear view of the defect structure and (c) Bader charges on the atoms near the defect.

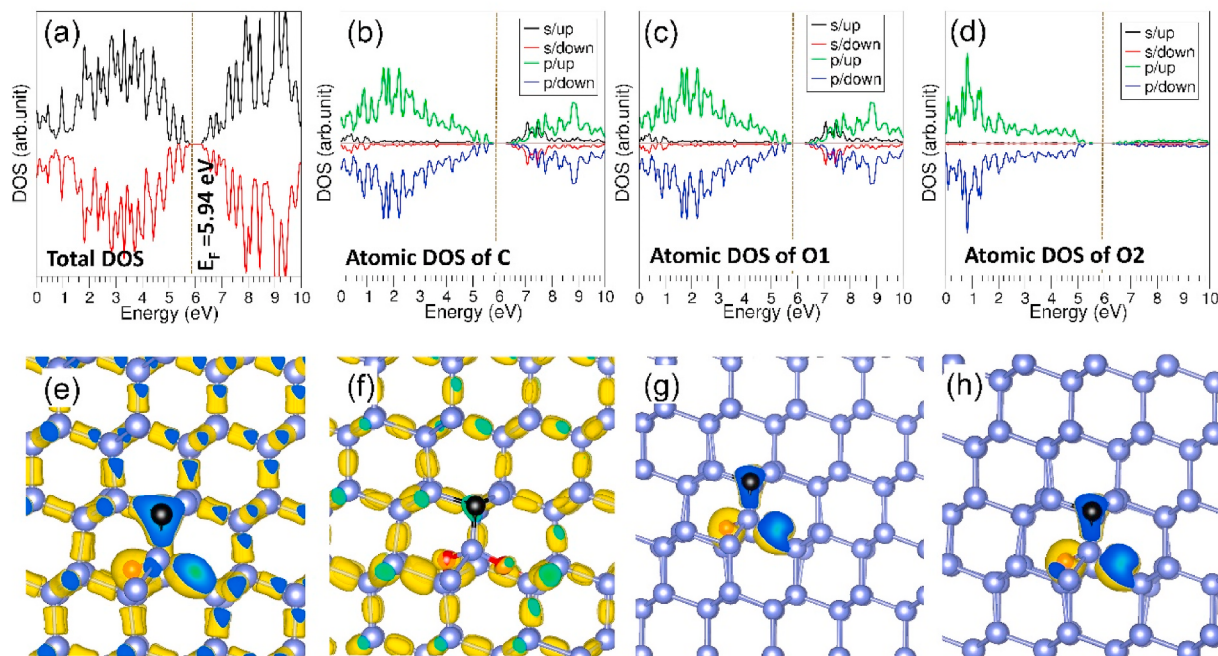


Fig. 5. (a) Total DOS plot, (b) atomic DOS plot of C, (c) atomic DOS plot of O₁, (d) atomic DOS plot of O₂, (e) total charge density plot; band decomposed charge density plots associated with (f) C, (g) O₁ and (h) O₂. Charge density plots were constructed using an isosurface value of 0.06.

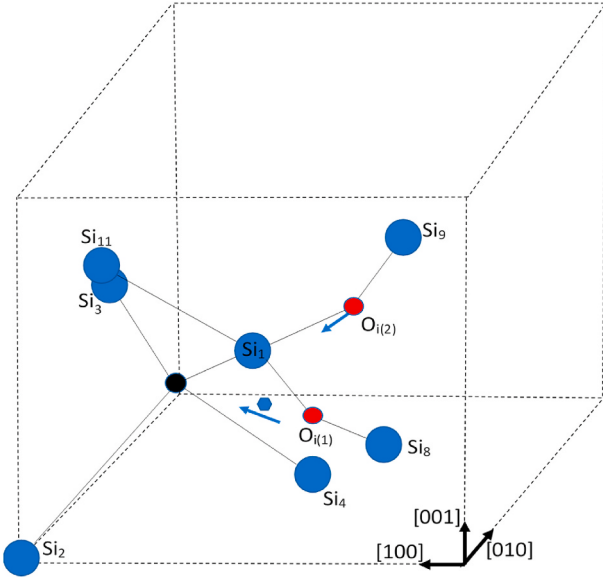


Fig. 6. Schematic representation of the CsO_{2i} configuration in the unit cell. Blue, black and red circles correspond to silicon, carbon and oxygen atoms. Small blue hexagon is for the reduced mass, μ . Blue arrows indicate the oscillation directions of the $\text{CsO}_{i(1)}$ and the $\text{O}_{i(2)}$ dipoles.

dipole moment of the cluster when the atoms were displaced in proportion to the normal coordinates [53]. Experimentally, the effective charge is determined by independent calibration to relate the concentration of the defect with the absorption strength of the LVM band [51]. The concentration N is measured with a variety of methods, as secondary ion mass spectroscopy (SIMS), Hall effect, activation analysis, etc. Then, they are connected with the corresponding absorption coefficient a_{\max} of the defect band received by IR absorption measurements. From relation (3) between a_{\max} and N the value of the effective charge is obtained.

The effective charge of $\text{CsO}_{i(1)}$ attributed to the 1103 cm^{-1} oxygen-related line is concentrated on the $\text{CsO}_{i(1)}$ reduced mass μ , and is equal to $Z_{\text{CsO}_{i(1)}} = 3.0 |e|$ where $|e|$ is the electron charge [19,54]. The effective charge concentrated on the $\text{O}_{i(2)}$ atom is equal to $Z_{\text{O}_i} = 4.1 |e|$, where $|e|$ is the electron charge [19].

The procedure to evaluate the LVM frequencies of the CsO_{2i} defect utilizes a previously used method founded on the interaction of the $\text{CsO}_{i(1)}$ and $\text{O}_{i(2)}$ dipoles [55,56]. The force constant of the perturbed oscillating $\text{CsO}_{i(1)}$ entity is $K_{\text{CsO}_{i(1)}}$ and is given by the relation

$$K_{\text{CsO}_{i(1)}} = \mu(\omega_{\text{CsO}_{i(1)}})^2 \quad (4)$$

where $\omega_{\text{CsO}_{i(1)}}$ is the oxygen related LVM frequency of the $\text{CsO}_{i(1)}$ defect at 1103 cm^{-1} . Similarly, the force constant of the oscillating $\text{O}_{i(2)}$ atom, $K_{\text{O}_{i(2)}}$, is given by the relation

$$K_{\text{O}_{i(2)}} = m_o(\omega_{\text{O}_{i(2)}})^2 \quad (5)$$

and corresponds to the $\omega_{\text{O}_{i(2)}} = 1107 \text{ cm}^{-1}$ LVM frequency of the oxygen interstitial atom [8].

We adopt the C-μ direction for the oscillation of the reduced mass of the $\text{CsO}_{i(1)}$ dipole and the Si₁–Si₉ direction for the oscillation of the $\text{O}_{i(2)}$ dipole [52].

The formulae for the dipole moments $\mathbf{p}_{\text{CsO}_{i(1)}}$ and $\mathbf{p}_{\text{O}_{i(2)}}$ become

$$\mathbf{p}_{\text{CsO}_{i(1)}} = Z_{\text{CsO}_{i(1)}} q_1 \hat{\mathbf{q}}_1, \mathbf{p}_{\text{O}_{i(2)}} = Z_{\text{O}_{i(2)}} q_2 \hat{\mathbf{q}}_2 \quad (6)$$

where $\hat{\mathbf{q}}_1, \hat{\mathbf{q}}_2$ are the unit vectors along the oscillation directions of the dipoles. The potential energy of the interacting dipole moments is given by

$$U_{\text{int}} = \frac{1}{d_{\mu-O_{i(2)}}^3} \left[\mathbf{p}_{\text{CsO}_{i(1)}} \cdot \mathbf{p}_{\text{O}_{i(2)}} - 3 \left(\hat{\mathbf{n}} \cdot \mathbf{p}_{\text{CsO}_{i(1)}} \right) \left(\hat{\mathbf{n}} \cdot \mathbf{p}_{\text{O}_{i(2)}} \right) \right] \quad (7)$$

where $\hat{\mathbf{n}}$ is the unit vector along the direction that connects the two dipoles and $d_{\mu-O_{i(2)}} = 2.28 \text{ \AA}$ is the distance between them [57]. The motion of the two dipoles is described by the effective Hamiltonian

$$H = \frac{1}{2} \mu \ddot{q}_1^2 + \frac{1}{2} m_o \ddot{q}_2^2 + \frac{1}{2} K_{\text{CsO}_{i(1)}} q_1^2 + \frac{1}{2} K_{\text{O}_{i(2)}} q_2^2 + \lambda q_1 q_2 \quad (8)$$

By comparing Eqs. (7) and (8) we obtain the q-independent part λ , to be equal to $\lambda = 51.5 \text{ J/m}^2$. The Hamiltonian of Eq. (8) has two normal modes with frequencies

$$\omega_{\text{CsO}_{2i}} = \sqrt{\frac{1}{2} \left[\omega_{\text{CsO}_{i(1)}}^2 + \omega_{\text{O}_{i(2)}}^2 \pm \sqrt{(\omega_{\text{CsO}_{i(1)}} - \omega_{\text{O}_{i(2)}})^2 + \frac{4 \lambda^2}{\mu \cdot m_o}} \right]} \quad (9)$$

where “+” preceding the inner square root corresponds to the antisymmetric normal mode and “-” to the symmetric one. By substituting $\omega_{\text{CsO}_{i(1)}} = 1103 \text{ cm}^{-1}$ and $\omega_{\text{O}_{i(2)}} = 1107 \text{ cm}^{-1}$ in Eq. (9), we find $\omega_{\text{CsO}_{2i}}^{(\text{ant})} = 1140.1 \text{ cm}^{-1}$ and $\omega_{\text{CsO}_{2i}}^{(\text{sym})} = 1064.7 \text{ cm}^{-1}$.

The frequency at 1064.7 cm^{-1} , corresponding to the symmetric vibrational mode related to the 1103 cm^{-1} oxygen-related mode of the CsO_i defect [7] matches well (deviation by $\sim 1.6\%$) the detected line in our spectra at 1048 cm^{-1} , as well as the lines at 1048 cm^{-1} (room-temperature) and 1052 cm^{-1} (low-temperature), reported at earlier studies [26,33,36]. The frequency at 1140.1 cm^{-1} , corresponding to the antisymmetric mode of the CsO_{2i} related to the same oxygen-related LVM at 1103 cm^{-1} of the CsO_i defect, also lies in the immediate vicinity of the experimentally detected line correlated with the CsO_{2i} defect at 1094 cm^{-1} (room-temperature) and 1099 cm^{-1} (low-temperature) (deviation by $\sim 4.2\%$) [26,33,36]. However, any signal from the 1094 cm^{-1} band, in our studies at room-temperature, was probably masked by the intense signal of the O_i band in the range 1050 – 1200 cm^{-1} and could not be detected. The above results enhance the assignment of the 1048 cm^{-1} to the CsO_{2i} defect.

4. Conclusions

To summarize, the aim of the present study has been the investigation of the CsO_{2i} defect in Si. Density functional theory (DFT) calculations have been performed to find the most energetically favorable structures of oxygen di-interstitials near a carbon substitutional atom in silicon (CsO_{2i}). The application of DFT technique has allowed us to analyze the interaction of oxygen di-interstitials with carbon and to calculate the amount of charges on the atoms near the defects. Afterwards, the dipole-dipole interaction method has been employed to calculate the Local Vibrational Mode (LVM) frequencies related with the most probable structure of the CsO_{2i} defect, as suggested by DFT. Two bands at 1064.7 and 1140.1 cm^{-1} have been estimated. These values are in agreement with the experimental values at 1048 and 1094 cm^{-1} , previously reported in the literature. Next, Infrared spectroscopy (IR) measurements carried out at Room Temperature (RT) have detected a band at 1048 cm^{-1} raised in the spectra upon annealing out of the two bands of the vacancy-oxygen (VO) and the carbon interstitial-oxygen interstitial (C_iO_i) defects. The behavior of this band, its formation temperature and its thermal evolution have strongly suggested correlation with the CsO_{2i} defect. The other band of the structure at 1094 cm^{-1} has not been detected in this study of RT measurements, probably because its weak signal has been masked by the very strong band of oxygen interstitial (O_i) at 1107 cm^{-1} . This study on the structure and properties of the CsO_{2i} defect has been expected to lead to further experimental and theoretical work on higher order carbon-oxygen defects that are important for Si based devices.

Data availability statement

The data that supports the findings of this study are available from the corresponding author upon reasonable request.

Declaration of competing interest

The authors declare that they have no known competing financial

interests or personal relationships that could have appeared to influence the work reported in this paper.

Acknowledgments

T. Angeletos would like to thank A. S. Onassis Foundation for financial support for his Ph. D. thesis through scholarship (Grant No. G ZL 001-1/2015-2016).

Appendix

Table I
Selected bond distances and bond angles in the relaxed structure of a single C-doped silicon.

Type of bond	Bond distance (Å)
Si ₁ -C	2.02
Si ₂ -C	2.02
Si ₃ -C	2.01
Si ₄ -C	2.01
Si ₁ -Si ₈	2.40
Si ₁ -Si ₉	2.40
Si ₁ -Si ₁₁	2.40
Si ₂ -Si ₅	2.41
Si ₅ -Si ₆	2.35
Si ₆ -Si ₇	2.35
Si ₄ -Si ₇	2.40
Si ₉ -Si ₁₀	2.35
Type of angle	Bond angle (°)
Si ₁ CSi ₂	109.53
Si ₁ CSi ₃	109.45
Si ₁ CSi ₄	109.40
Si ₂ CSi ₃	109.44
Si ₂ CSi ₄	109.47
Si ₈ Si ₁ Si ₉	102.54
Si ₈ Si ₁ Si ₁₁	102.72
Si ₉ Si ₁ Si ₁₁	102.66

References

- [1] A. Alkauskas, M.D. McCluskey, C.G. Van de Walle, *J. Appl. Phys.* 119 (2016) 181101.
- [2] M. Stavola, W. Beall Fowler, *J. Appl. Phys.* 123 (2018) 161561.
- [3] H.M. Ayedh, E.V. Monakhov, J. Coutinho, *Phys. Rev. Mater.* 4 (2020), 064601.
- [4] A. Chroneos, E.N. Sgourou, C.A. Londos, U. Schwingenschlögl, *Appl. Phys. Rev.* 2 (2015), 021306.
- [5] D. Timerkaeva, D. Caliste, T. Deutsch, P. Pochet, *Phys. Rev. B* 96 (2017) 195306.
- [6] P. Dong, X.G. Yu, L. Chen, X.Y. Ma, D.R. Yang, *J. Appl. Phys.* 122 (2017), 095704.
- [7] G. Davies, R.C. Newman, *Handbook on Semiconductors, Materials Properties and Preparations*, Edited by T. S. Moss and S. Mahajan (North Holland, Amsterdam, 1994, p. 1557).
- [8] R.C. Newman, R. Jones, *Oxygen in Silicon, Semiconductors and Semimetals*, in: F. Shimura (Ed.) vol. 42, Academic press, Orlando, 1994, p. 289.
- [9] R.C. Newman, *Infrared studies of crystal defects* (taylor and francis, london, 1973).
- [10] B. Pajot, B. Clerjaud, *Optical Absorption of Impurities and Defects in Semiconducting Crystals. II. Electronic Absorption of Deep Centres and Vibrational Spectra*, Springer-Verlag, Berlin, 2013.
- [11] A. Borghesi, B. Pivac, A. Sassella, A. Stella, *J. Appl. Phys.* 77 (1995) 4169.
- [12] H. Bender, J. Vanhellemont, *Handbook on Semiconductors*, in: S. Mahajan (Ed.), Elsevier Science B.V., North Holland, 1994 vols. 3b, 1637.
- [13] W. Skorupa, R.A. Yankov, *Mater. Chem. Phys.* 44 (1996) 101.
- [14] C.A. Londos, M.S. Potsidi, V.V. Emtsev, *phys. stat. sol. (c)* 2 (2005) 1963.
- [15] G.D. Watkins, J.W. Corbett, *Phys. Rev.* 121 (1961) 1001.
- [16] B.G. Svensson, J.L. Lindström, *phys. stat. sol. (a)* 95 (1987) 537.
- [17] C.A. Londos, *phys. stat. sol. (a)* 102 (1987) 639.
- [18] C.A. Londos, *phys. stat. sol. (a)* 92 (1985) 609.
- [19] S.P. Chappell, M. Claybourn, R.C. Newman, K.G. Barracough, *Semicond. Sci. Technol.* 3 (1988) 1047.
- [20] G. Ferenczi, C.A. Londos, T. Pavelka, M. Somogyi, *J. Appl. Phys.* 63 (1988) 183.
- [21] D. Tsuchiya, K. Sueoka, H. Yamamoto, *Phys. Status Solidi A* 1800615 (2019).
- [22] S.D. Brotherton, P. Bradley, *J. Appl. Phys.* 53 (1982) 5720.
- [23] M. Siemieniec, F.-J. Niedernostheide, H.-J. Schlze, W. Sudkamp, U. Kellner-Werdehausen, J. Lutz, *J. Electrochem. Soc.* 153 (2006) G108.
- [24] P. Pichler, in: S. Selberherr (Ed.), *Intrinsic Point Defects, Impurities and Their Diffusion in Silicon*, Springer Verlag, Wien, 2004.
- [25] R.C. Newman, R.S. Smith, *J. Phys. Chem. Solid.* 30 (1969) 1493.
- [26] H. Yamada-Kaneta, Y. Shirakawa, C. Kaneta, *Early Stages of Oxygen Precipitation in Silicon*, in: R. Jones (Ed.), Kluwer Academic Publishers, Netherlands, 1996, pp. 389–396.
- [27] Y. Shirakawa, H. Yamada-Kaneta, 80, 4199 (1996).
- [28] C. Kaneta, T. Sasaki, H. Katayama-Yoshida, *Mater. Sci. Forum* 117–118 (1993) 81.
- [29] C.A. Londos, E.N. Sgourou, A. Chroneos, V.V. Emtsev, *Semicond. Sci. Technol.* 26 (2011) 105024.
- [30] N. Inoue, H. Ohyama, Y. Goto, T. Sugiyama, *Physica B* 401–402 (2007) 477.
- [31] C.A. Londos, A. Andrianakis, E.N. Sgourou, V.V. Emtsev, H. Ohyama, *J. Appl. Phys.* 109 (2011), 033508.
- [32] C.A. Londos, E.N. Sgourou, D. Timerkaeva, A. Chroneos, P. Pochet, V.V. Emtsev, *J. Appl. Phys.* 114 (2013) 113504.
- [33] L.I. Murin, V.P. Markevich, J.L. Lindstrom, M. Kleverman, J. Hermansson, T. Hallberg, B.G. Svensson, *Solid State Phenom.* 82–84 (2002) 57.
- [34] L.I. Murin, V.A. Gurinovich, I.F. Medvedeva, V.P. Markevich, *Inorg. Mater.: Applied Research* 7 (2016) 192.
- [35] P. Chen, X. Yu, X. Liu, X. Chen, Y. Wu, D. Yang, *Appl. Phys. Lett.* 102 (2013), 082107.
- [36] N. Inoue, T. Sugiyama, Y. Goto, K. Watanabe, H. Seki, Y. Kawamura, *phys. stat. solidi C* 13 (2016) 883.
- [37] G. Kresse, J. Furthmüller, *Phys. Rev. B* 54 (1996) 11169.
- [38] G. Kresse, D. Joubert, *Phys. Rev. B* 59 (1999) 1758–1775.
- [39] P.E. Blöchl, *Phys. Rev. B* 50 (1994) 17953–17979.
- [40] J.P. Perdew, K. Burke, M. Ernzerhof, *Phys. Rev. Lett.* 77 (1996) 3865–3868.
- [41] H.J. Monkhorst, J.D. Pack, *Phys. Rev. B* 13 (1976) 5188–5192.
- [42] W.H. Press, S.A. Teukolsky, W.T. Vetterling, B.P. Flannery, *Numerical Recipes in C* (2nd ed.): the Art of Scientific Computing, Cambridge University Press., 1992.
- [43] R.F.W. Bader, *Theoretical Chemistry Accounts* 105 (2001) 276–283.
- [44] S. Grimm, J. Antony, S. Ehrlich, H. Krieg, *J. Chem. Phys.* 132 (2010) 154104.
- [45] A. Chroneos, *J. Appl. Phys.* 105 (2009), 056101.
- [46] A. Chroneos, C. Jiang, R.W. Grimes, U. Schwingenschlögl, H. Bracht, *Appl. Phys. Lett.* 95 (2009) 112101.
- [47] A. Chroneos, H. Bracht, R.W. Grimes, B.P. Uberuaga, *Mater. Sci. Eng. B* 154–155 (2008) 72.
- [48] A. Chroneos, D. Skarlatos, C. Tsamis, A. Christofi, D.S. McPhail, R. Hung, *Mater. Sci. Semicond. Process.* 9 (2006) 640–643.
- [49] C.A. Londos, D.N. Aliprantis, G. Antonaras, M.S. Potsidi, T. Angeletos, *J. Appl. Phys.* 123 (2018) 145702.

- [50] D.R. Lide, CRC Handbook of Chemistry and Physics: A Ready-Reference Book of Chemical and Physical Data/, 82nd ed., CRC, Boca Raton, 2004. Web.
- [51] M. Stavola, Vibrational Spectroscopy of Light impurities in Semiconductors, Charter 3 in: Semiconduct. Semimet. 51B (1999) 153.
- [52] M.D. Mc Cluskey, Appl. Phys. Rev. 87 (2000) 3593.
- [53] R. Jones, A. Umerski, S. Oberg, Phys. Rev. B 45 (1992) 11321.
- [54] G. Davies, A.S. Oates, R.C. Newman, R.A. Woolley, E.C. Lightowers, M.J. Binns, J. G. Wilkes, J. Phys. C Solid State Phys. 19 (1986) 841.
- [55] N.V. Sarlis, C.A. Londos, L.G. Fytros, J. Appl. Phys. 81 (1997) 1645.
- [56] M.S. Potsidi, C.A. Londos, J. Appl. Phys. 100 (2006), 033523.
- [57] J. Jackson, Classical Electrodynamics, Wiley, New York, 1975, p. 136.